Real-Time, Model-Based Spray-Cooling Control System for Steel Continuous Casting

BRYAN PETRUS, KAI ZHENG, X. ZHOU, BRIAN G. THOMAS, and JOSEPH BENTSMAN

This article presents a new system to control secondary cooling water sprays in continuous casting of thin steel slabs (CONONLINE). It uses real-time numerical simulation of heat transfer and solidification within the strand as a software sensor in place of unreliable temperature measurements. The one-dimensional finite-difference model, CON1D, is adapted to create the real-time predictor of the slab temperature and solidification state. During operation, the model is updated with data collected by the caster automation systems. A decentralized controller configuration based on a bank of proportional-integral controllers with antiwindup is developed to maintain the shell surface-temperature profile at a desired set point. A new method of set-point generation is proposed to account for measured mold heat flux variations. A user-friendly monitor visualizes the results and accepts set-point changes from the caster operator. Example simulations demonstrate how a significantly better shell surface-temperature control is achieved.

DOI: 10.1007/s11663-010-9452-7

I. INTRODUCTION

IN continuous casting of steel, robust and accurate control of secondary cooling is vital to the production of high-quality slabs.[1] Defects such as transverse surface cracks form unless the temperature profile down the caster is optimized to avoid stress, such as unbending, during temperature regions of low ductility.[2] This is especially important in thin-slab casters because high casting speed and a tight machine radius exacerbate cracking problems and because surface inspection to detect defects is difficult. Thus, great incentive exists to implement control systems to optimize spray cooling to maintain desired temperature profiles.

Secondary cooling presents several control challenges. Conventional feedback control systems based on hardware sensors have not been successful because emissivity variations from intermittent surface scale and the harsh environment of the steam-filled spray chamber make optical pyrometers unreliable. Thin-slab casting is particularly difficult because the high casting speed requires faster response. Modern air-mist cooling nozzles offer the potential advantages of faster and more uniform cooling but introduce the extra challenge of air flow rate as another process variable to control. Most casters control spray-water flow rates using a simple look-up table with casting speed. This produces undesirable temperature transients during process changes, so recent dynamic control systems have been developed based on real-time computational models. However, their application to thin-slab casting has been prevented by the short response times needed and the increased relative importance of solidification in the mold, which is not easy to predict accurately.

Several previous attempts have been made to implement real-time dynamic control of cooling of continuous casters. It has been recognized for a long time that the spray-water flow should be adjusted so that each portion of the strand surface experiences the same desired thermal history. This is especially important, and not always intuitive, during and after transients such as casting slowdowns during ladle exchanges. Okuno *et al.*[3] and Spitzer *et al.*[4] each proposed real-time model-based systems to track the temperature in horizontal slices through the strand to maintain surface temperature at four to five set points. Computations were performed every 20 seconds and online feedback-control sensors calibrated the system. In practice, these systems have been problematic, owing to the unreliability of temperature sensors such as optical pyrometers.

Barozzi *et al.* developed a system to control both spray cooling and casting speed dynamically at the same time.[5] Feedforward control was used to allow the predicted temperatures to match the set points, but their heat flow model was relatively crude, owing to the slow computer speed of that time. Optimizing spray cooling to avoid defects using fundamentally based computational models was proposed by Lally.[6] At that time, the slow computer speed and inefficient fundamental computational models and control algorithms made online control infeasible.

In recent years, several open-loop model-based control systems have been developed to control spray-water

BRYAN PETRUS, KAI ZHENG, X. ZHOU, Graduate Research Assistants, BRIAN G. THOMAS, Gauthier Professor, and JOSEPH BENTSMAN, Professor, are with the Department of Mechanical Science and Engineering, University of Illinois, Urbana, IL 61801. Contact e-mail: bgthomas@uiuc.edu

Manuscript submitted July 14, 2009.
Article published online December 7, 2010.

cooling under transient conditions for conventional thick-slab casters. These systems employ online computational models to ensure that each portion of the shell experiences the same cooling conditions. Spray-water flow rates have been controlled in a thick slab caster using a one-dimensional (1-D) finite difference model[7] that updates about once every minute. Hardin *et al.*[8] and Louhenkilpi *et al.*[9–11] have developed two-dimensional (2-D) and three-dimensional (3-D) heat flow models for the online control of spray cooling. One model, DYN3D, uses steel properties and solid fraction–temperature relationships based on multicomponent phase diagram computations.[11] Another model, DYNCOOL, has been used to control spray cooling at Rautaruukki Oy Raahe Steel Works.[12]

Although these model-based control systems are significant achievements, none of the models are robust enough for general use. Each must be tuned extensively on an individual caster, owing to nongeneral heat-transfer coefficients and the use of *ad hoc* heuristic methods rather than rigorous control algorithms. None of the previous models uses sensor data input for the mold water cooling, which is readily available and reliable. Finally, none of these models has been applied to a thin-slab caster, which has the control problems associated with higher speed and where cooling in the mold is more important.

This article presents a new real-time control system, briefly introduced first in References 13 and 14, called CONONLINE, that has been developed to control spray cooling in thin-slab casters and recently has been implemented at the Nucor Steel casters in Decatur, Alabama. This system features an efficient fundamentally based solidification heat-transfer model of a longitudinal slice through the strand as a "software sensor" of surface temperature. This model, CONSENSOR, estimates the entire shell surface temperature and solidification profile in real time, based on tracking multiple horizontal slices through the strand with a subroutine version of a previous computational model (CON1D).[15] The empirical coefficients in the model previously were calibrated to match offline pyrometer measurements in the specific caster. Then, ten independently tuned proportional-integral (PI) controllers together with classical antiwindup[16] are designed to maintain the shell surface-temperature profile at the desired set points in each of the ten spray cooling zones throughout changes in casting speed, steel grade, and other casting conditions.

An important feature of this system is that CONSENSOR performs closed-loop estimation in the mold and open-loop estimation in the secondary cooling (spray) zones. Loop closure at the mold exit (beginning of secondary cooling) is attained by matching the total heat removal in the mold with the measured temperature increase of the mold cooling water. As described in more detail in Section IV–D, this makes CONSENSOR a *hybrid* strand temperature observer. At present, fully closed-loop control is not possible because of the unreliability of temperature sensing in the secondary cooling region. Even with reliable pyrometers, open-loop model-based estimation likely still would be needed to fill the gaps between their highly localized readings to attain reasonable control performance.

In addition to the software sensor and the controller, this real-time spray-cooling control system also includes a monitor interface to provide real-time visualization of the shell surface-temperature predictions, the predicted metallurgical length, spray-water flow rates, set points, and other information important to the operator, as well as to allow operator input through the choice of temperature set points. The system uses shared memory and TCP/IP server and client routines for communication among the software sensor, controller, monitor interface, and the caster automation systems. Simulation results demonstrate that significantly better shell surface-temperature control is achieved.

II. CONTROL SYSTEM OVERVIEW

The new dynamic control system for thin-slab casters is based on the control diagram shown in Figure 1. The core of the system is a software sensor based on the CON1D heat-conduction model. The software sensor, CONSENSOR, provides a real-time estimate/prediction of the strand state, including the shell surface-temperature distribution and metallurgical length. It updates based on all the available casting conditions, which include the following: (1) conditions updated every second, including mold heat flux, casting speed, pour temperature (for superheat), strand width, and spray flow rates; (2) the heat-specific steel composition that is updated for heat changes during ladle exchanges; and (3) conditions updated only when the software sensor is calibrated, including the mold, roll, and spray nozzle configurations, parameters in the heat-transfer coefficient models, and strand thickness. The estimated shell temperature profile then is compared against a predetermined surface-temperature profile set point, which also varies with casting conditions such as mold heat flux, as described later. The mismatch between the estimate and the set point (*i.e.*, the tracking error) then is sent to a dynamic controller to compute the water flow rate command required to drive the mismatch to zero. Finally, the computed command set of spray-water flow rates is sent to the spray zone actuators in the operating caster, to the monitor program for visual display to caster operator, as well as to the software sensor for estimation at the next second.

III. SYSTEM ARCHITECTURE AND IMPLEMENTATION

The control diagram in Figure 1 is realized in CONONLINE, which consists of several programs running in real time on several different linked computers. As shown in Figure 2, the main system hardware consists of two powerful workstations with dual Intel Xeon Processors (Intel Corp., Santa Clara, CA) with two gigabytes of memory each. The "Model" workstation runs the software sensor CONSENSOR on the CentOS operating system (www.centos.org). The "Controller"

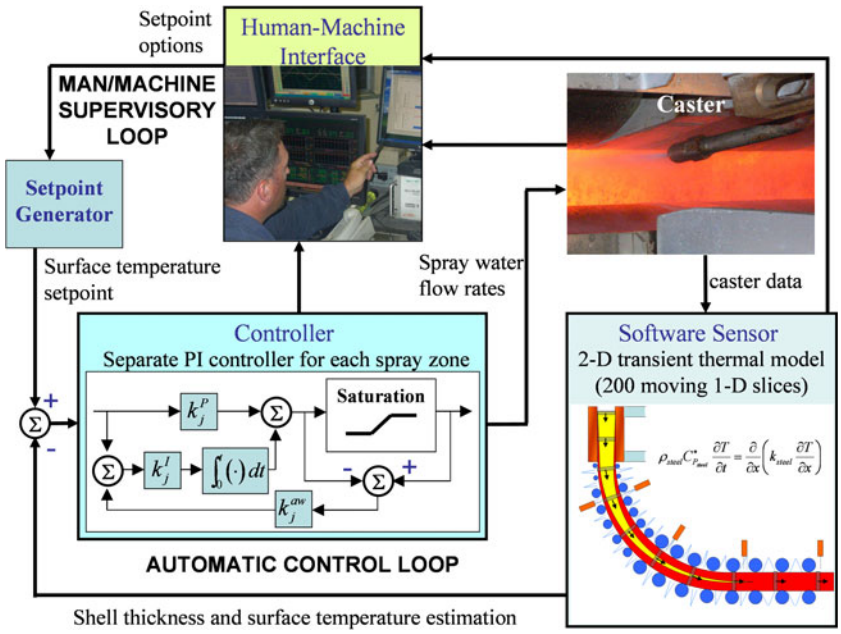

Fig. 1—Software sensor-based control diagram.

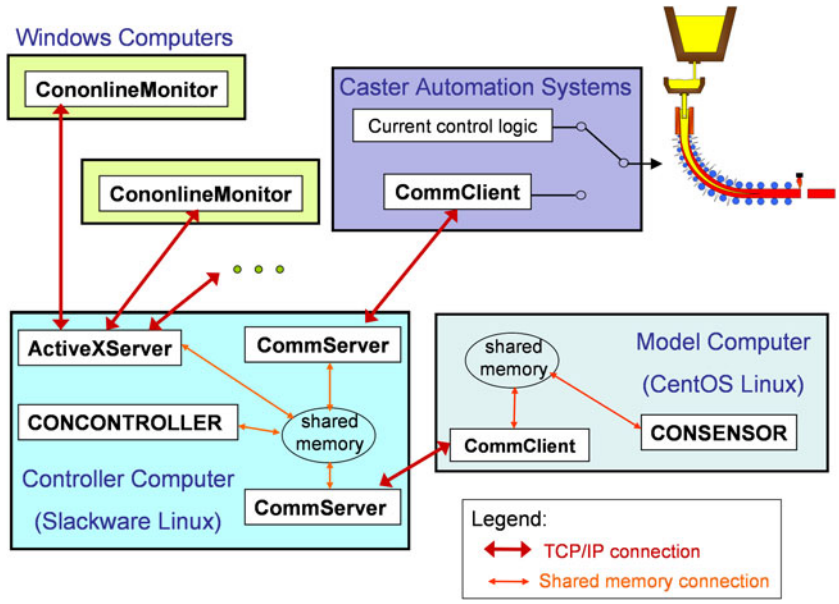

Fig. 2—Software sensor-based control system architecture.

workstation runs the controller, CONCONTROLLER on the Slackware Linux operating system (slackware.com). The various programs communicate through "shared memory," which is a block of memory with the same contents on each computer that is accessible by any program and is updated continuously *via* TCP/IP CommServer and CommClient. A separate TCP server C program (ActiveXServer) transmits the information to up to 16 Windows personal computers (PCs) running a human-interface Visual C++ monitor program. The monitor program displays the results and accepts user input while running simultaneously on several different computer screens. The CONSENSOR model is a FORTRAN program, owing to its computational efficiency. These programs are listed in Table I.

The control system in Figure 2 has the following operation modes, shown in the "Caster Automation Systems" block: (1) shadow mode, which displays the caster status and model predictions in which sprays are controlled using current control logic and (2) control mode, which also controls the caster *via* the CommClient software when it is switched on. Shadow mode allows the control system to be tested and tuned using real caster data, whereas the old controller controls the

Table I. Software Programs in the Control System

Program Name	Function
CONSENSOR	estimating/predicting the profile of shell temperature and thickness based on CON1D
CONCONTROLLER	computing the required spray water flow rate to maintain temperature set point
CONONLINE Monitor	displaying in real-time shell surface-temperature, thickness profile estimates/predictions, computed water flow rate, and casting conditions
TCP/IP server	working with TCP/IP client programs to transfer data between workstations
TCP/IP client	working with TCP/IP server programs to transfer data between workstations
ActiveXServer	TCP server working with monitor programs to transfer data between controller workstation and PCs running CONONLINE Monitor

secondary cooling in the actual caster. During shadow mode operation, many causes of crashes and errors were identified and solved, with the help of checks to ensure that input data stay within reasonable bounds. The system is now robust and maintains stable operation through all sets of conditions tested, including serious disruptions or errors in input data.

In either mode, the caster automation systems send casting conditions, discussed in Section IV, at each second to the Controller workstation *via* the TCP/IP client. The casting conditions are received by the TCP/IP server in the Controller workstation and relayed to the Model workstation *via* its client. These data are available immediately to the sensor and controller *via* the shared memory in each workstation. The software sensor then estimates the shell temperature distribution in ~0.5 seconds. The controller reads this distribution from shared memory and computes the spray-water flow rates to maintain the selected set points every second. To ensure timely updating, data in each shared memory are exchanged ~10 times per second with transmissions <20 ms each.

The predicted shell surface temperature and shell thickness profiles are transmitted *via* TCP/IP to up to 16 monitor programs to be displayed on the operator console and elsewhere in real time. The monitor program is updated every 3 seconds, which is slower than the 1-second controller updates to lessen transmission traffic on the steel mill general network. In control mode, the spray-water flow-rate commands also are sent to the caster automation systems to be applied in the flow actuators in the actual caster. Finally, changes to the temperature set points or control mode requested by the operator through the monitor are sent to the other computers in preparation for the next time increment.

IV. SYSTEM COMPONENTS

A. *Heat Transfer Model—CON1D*

CON1D is a simple but comprehensive fundamentally based model of heat transfer and solidification of the continuous casting of steel slabs, including phenomena in both the mold and the spray regions.[15] The accuracy of this model in predicting heat transfer with solidification has been demonstrated previously through comparison with analytical solutions of plate solidification and plant measurements.[15,17] Because of its accuracy, CON1D has been used by the steel industry to predict the effects of changes in casting conditions on solidification and to develop practices to prevent problems such as whale formation.[18]

The simulation domain in this work is a transverse slice through the strand thickness that spans from the shell surface at the inner radius to the outer radius surface. The CON1D model computes the complete temperature distribution within the solid, mushy, and liquid portions of the slice as it traverses the path from the meniscus down through the spray zones to the end of the caster at torch cutoff. CON1D uses an explicit central finite-difference algorithm to solve the following 1-D transient heat conduction equation within the solidifying steel shell[15]:

$$\rho_{\text{steel}} Cp^{*}_{\text{steel}} \frac{\partial T_i(x,t)}{\partial t} = k_{\text{steel}} \frac{\partial^2 T_i(x,t)}{\partial x^2} + \frac{dk_{\text{steel}}}{dT} \left(\frac{\partial T_i(x,t)}{\partial x} \right)^2 \quad [1]$$

where k_{steel} is thermal conductivity, ρ_{steel} is density, and Cp^{*}_{steel} is the effective specific heat of the steel, which includes the latent heat. The spatial dimension x extends through the entire thickness of the strand, perpendicular to the casting direction. To produce an estimate for the entire caster, the software sensor uses multiple simultaneous runs of CON1D; hence, the subscript i indicates the temperature history of a particular slice.

This Lagrangian formulation takes advantage of the high Peclet number of the continuous casting process, which renders axial heat conduction negligible.[15] The effect of nonuniform distribution of superheat is incorporated using the results from previous 3-D turbulent fluid flow calculations within the liquid pool.[15] Thermal properties vary with temperature according to composition-dependent phase fractions. Microsegregation effects are included *via* a modified Clyne–Kurz model.[15,19] Shell thickness is defined by a liquid fraction of 0.3. The latent heat of solidification is incorporated using an efficient enthalpy method and a posttime-step correction.[15] These solidification and thermal property models depend on the steel composition according to the amounts of the alloying elements included in Table II. Good accuracy is achieved using a grid spacing Δx of approximately 1 mm and finite-difference time-stepping size Δt_{FD} of 0.03 seconds. With this tool used as a subroutine by the software sensor, CONSENSOR, the closed-loop diagram of Figure 1 takes the form shown in Figure 3. The model box contains the explicit discretized form of Eq. [1] solved by

CON1D.[15] The initial condition is the pour temperature T_{pour}, measured in the tundish, and boundary conditions are summarized subsequently, with more detail provided elsewhere.[15]

1. *Boundary conditions in the mold*

A new method has been developed to define the surface heat flux profile accurately in the mold. In previous work, the CON1D model computes the surface heat flux within the mold region by solving a 2-D heat equation in the mold and several mass and heat balance equations within the interfacial gap.[15,20] Its accuracy in predicting mold heat transfer has been verified against a full 3-D finite element analysis, as well as plant measurements.[17]

For the present model, the average heat flux in the mold is found from the measured temperature increase and flow rate of the cooling water, which is supplied through the caster automation systems in real time. The surface heat flux profile down the mold, q_{mold} (MW/m^2), is fit with the following empirical function of time to match the average measured mold heat flux, $\bar{q}_{mold}(\mathrm{MW/m^2})$. This function is split into a linear portion and an exponential portion, which are written as follows:

$$-k_{steel}\frac{\partial T_i(\pm L,t)}{\partial x} = q_{mold}(t) = \begin{cases} q_0 - q_a \times \left(t - t_i^0\right), & 0 \le t - t_i^0 < t_c \\ q_b \times \left(t - t_i^0\right)^{-n}, & t_c < t - t_i^0 \le t_m \end{cases} \quad [2]$$

where t_i^0 is the start time for the slice; hence, $(t - t_i^0)$ is the time below meniscus and n is a fitting parameter that controls the shape of the curve, which was chosen to be 0.4. The initial heat flux q_0 is the maximum heat flux at the meniscus, which was expressed as follows:

$$q_0 = \bar{q}_{mold} \times q_{fac} \quad [3]$$

where q_{fac} is another parameter, set to 2.3. The total time spent in the mold t_m is calculated as follows:

$$t_m = \frac{z_m}{V_c} \quad [4]$$

where z_m is the mold length and V_c is the casting speed. The duration of the linear portion, t_c, is assumed to be expressed as follows:

$$t_c = t_m \times t_{fac} \quad [5]$$

where t_{fac} is a third parameter, set to 0.07. Then the intermediate parameters q_a and q_b are defined in the following equations and are based on keeping the curve continuous and matching the total mold heat flux in the mold with the area beneath the curve:

$$q_a = \frac{q_0 \times (t_c)^n (t_m)^{1-n} - (1-n) \times \bar{q}_{mold} \times t_m - n \times q_0 \times t_c}{t_c^{1+n} \times t_m^{1-n} - \frac{1}{2}(1+n)t_c^2} \quad [6]$$

$$q_b = q_0 \times (t_c)^n - q_a (t_c)^{n+1} \quad [7]$$

Table II. Simulated Steel Composition

Element	Symbol	Wt Pct
Carbon	p_C	0.24
Manganese	p_{Mn}	1.09
Sulfur	p_S	0.0019
Phosphorus	p_P	0.014
Silicon	p_{Si}	0.175
Chromium	p_{Cr}	0.04
Nickel	p_{Ni}	0.04
Copper	p_{Cu}	0.087
Molybdenum	p_{Mo}	0.01
Titatium	p_{Ti}	0.002
Aluminum	p_{Al}	0.039
Vanadium	p_V	0.001
Nitrogen	p_N	0.0076
Niobium	p_{Nb}	0.035

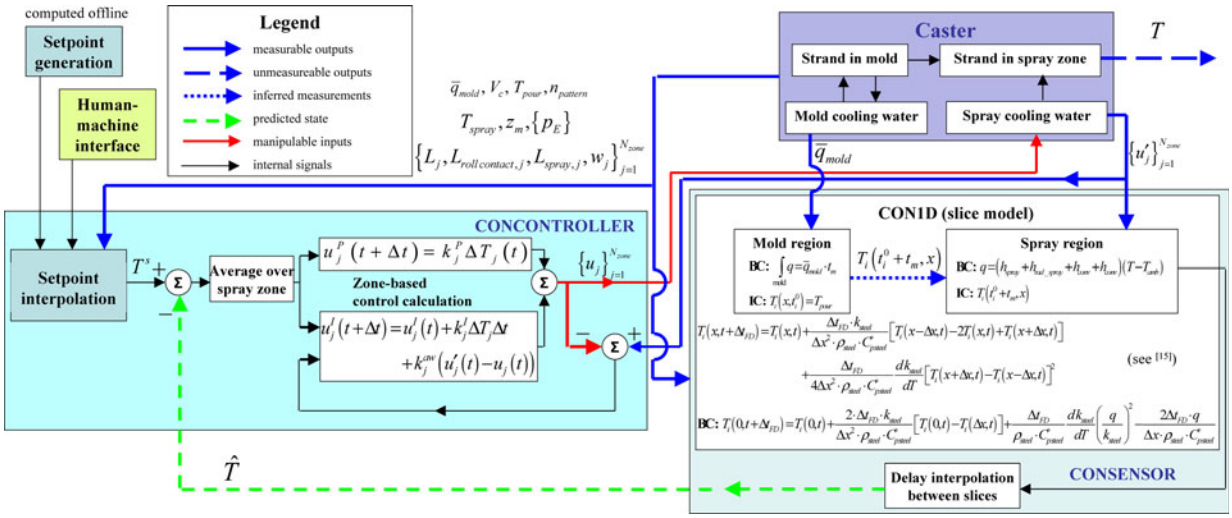

Fig. 3—Closed-loop diagram with CONSENSOR estimator/predictor and CONCONTROLLER control algorithm.

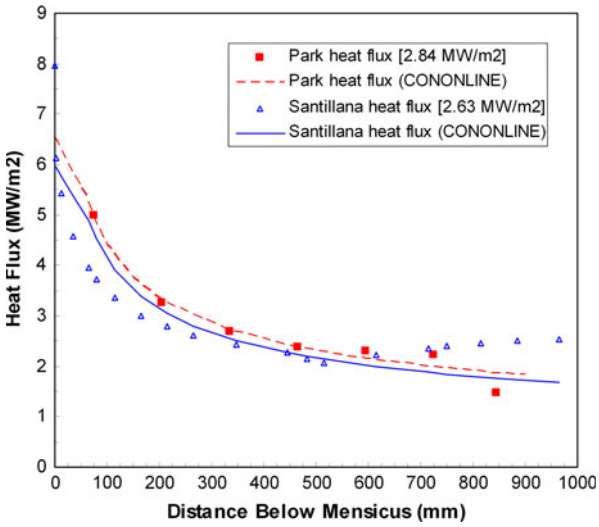

Fig. 4—Comparison of CONONLINE mold heat flux profiles from Eqs. [2] through [7] with measurements from Refs. 17 and 21.

Figure 4 compares heat flux profiles predicted with this new model to previous measurements in thin-slab casting molds.[17,21]

2. *Spray-zone boundary conditions*

Below the mold, heat flux from the strand surface is expressed as follows:

$$-k_{\text{steel}}\frac{\partial T_i(\pm L,t)}{\partial x} = h(T_i(\pm L,t) - T_{\text{amb}}) \qquad [8]$$

where T_{amb} is the ambient temperature and h (W/m^{2}K) varies greatly between each pair of support rolls according to components, including the following: spray nozzle cooling (based on water flux) h_{spray}, radiation $h_{\text{rad\_spray}}$, natural convection h_{conv}, and heat conduction to the rolls h_{roll}, as shown in Figure 5. Incorporating these phenomena enables the model to simulate heat transfer during the entire continuous casting process. Spray cooling heat extraction is specified as the following function of water flow rate[1]:

$$h_{\text{spray}} = A \times Q_{sw,j}^{c} \times \left(1 - b \times T_{\text{spray}}\right) \qquad [9]$$

where $Q_{sw,j}$ (l/m^{2}s, where l stands for liters) is the water flux in spray zone j and T_{spray} is the temperature of the spray cooling water (°C). For air-mist nozzles, this work assumes that air flows are consistent functions of water flow; hence they are not considered separately.

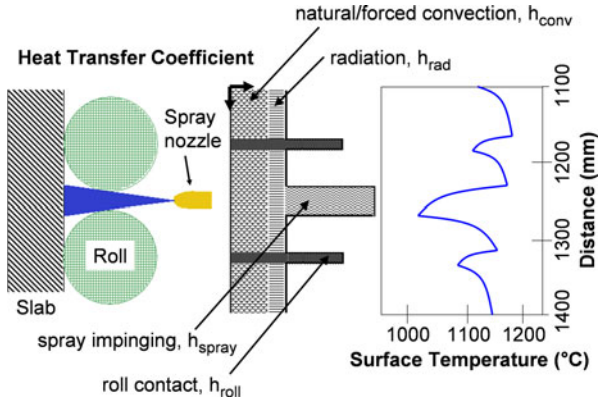

Fig. 5—Schematic of spray zone region.

used successfully by other modelers.[1,22,23] Others describe the variation of heat flux with nozzle type, nozzle-to-nozzle spacing, spray-water flow rate, and distance of the spray nozzles from the strand surface, based on plant and lab studies.[1,24,25] Recent experimental work aims to develop more fundamental heat-transfer relationships for spray cooling, based on droplet size and impact,[26,27] including studies of air mist cooling.[27,28] This work combines previous correlations with recent lab measurements of the spray patterns obtained from the nozzles used in the caster of interest in this work.[29,30] To improve fundamental prediction of spray-zone heat extraction, experimental measurements using a new steady-state apparatus are being conducted.[31] The well-known drop in heat extraction from the sprays on the bottom surface of the strand, and the increase in heat extraction caused by the Leidenfrost effect at lower temperatures, both can be accommodated, but await these measurements.

Radiation, $h_{\text{rad\_spray}}$ is calculated as follows:

$$h_{\text{rad\_spray}} = \sigma \times \varepsilon_{\text{steel}}\left(T_{i,sK} + T_{\text{amb K}}\right)\left(T_{i,sK}^2 + T_{\text{amb K}}^2\right) \qquad [10]$$

where $T_{i,sK}$ is the surface temperature of the strand, $T_i(\pm L,t)$, expressed in Kelvin, σ is the Stefan–Boltzman constant (5.67×10^{-8} W/m^{2}K^4), and $\varepsilon_{\text{steel}}$ is the emissivity of the strand surface, 0.8, and $T_{\text{amb K}}$ is the ambient temperature, 298 K (25 °C). Natural convection is not important, so it is treated here as a constant 8.7 W/m^{2}K. The heat-transfer coefficient extracting heat into each roll h_{roll} is expressed as a fraction of the total heat extracted to the rolls f_{roll}, which is calibrated as follows for each spray zone[15]:

$$h_{\text{roll}} = \frac{\left(h_{\text{rad\_spray}} + h_{\text{conv}} + h_{\text{spray}}\right) \times L_{\text{spray},j} + \left(h_{\text{rad\_spray}} + h_{\text{conv}}\right) \times \left(L_j - L_{\text{spray},j} - L_{\text{roll contact},j}\right)}{L_{\text{roll contact},j} \times \left(1 - f_{\text{roll},j}\right)} \times f_{\text{roll},j} \qquad [11]$$

Finding parameters to predict spray cooling heat extraction accurately presents a significant challenge that has been the focus of several previous experimental studies. In Nozaki's empirical correlation,[22] $A = 0.3925$, $c = 0.55$, and $b = 0.0075$, which has been

This fraction can be based on the measured water temperature increase of roll cooling water augmented with some external sprays. Increasing f_{roll} increases the severity of local temperature drops beneath the rolls. Severity also depends on the length of the roll contact

region, $L_{\text{rollcontact}}$, based here on assuming a contact angle with the roll of 10 deg. Beyond the spray zones, heat transfer simplifies to radiation and natural convection.

3. *Model calibration and example results*

CON1D has been validated with plant measurements in the spray zones on several different operating slab casters.[15,17,18] This versatile modeling tool has been applied to a wide range of practical problems in continuous casters. For the current work, the model was calibrated to match the average surface temperatures measured under steady-state conditions using five Modline 5 pyrometers (Ircon, Santa Cruz, CA) installed along the south Nucor caster in Decatur, Alabama in January 2006. Each pyrometer was centered between two neighboring rolls and between spray nozzles with an approximate stand-off distance of 203 mm from the strand surface, as shown in Figure 6. They were located 3866 mm, 6015 mm, 8380 mm, 11385 mm, and 13970 mm, from the meniscus. The temperature was converted using linear transformation of the voltage signal and averaged over 450 seconds. Each measurement was estimated to average over a 15-mm diameter spot.

A typical example of the steady-state experiments is given here to demonstrate the calibration. A 90-mm thick × 1396-mm wide thin slab of low carbon steel was cast at 3.61 m/min. The steel composition is given in Table II. The pour temperature was 1821 K (1548 °C), and the average mold heat removal was 2.4243 MW/m^2. The average spray-water flow rates and details on the roll and caster dimensions are given in Table III and elsewhere.[32] The average pyrometer temperatures with error bars to indicate the standard deviation are shown in Figure 7(a) together with the strand outer surface-temperature profile predicted by CON1D. The dips in the temperature profile are caused by roll contact and spray cooling, whereas the temperature peaks occur where convection and radiation are the only mechanisms of heat extraction. Dips and peaks are shown clearly in Figure 7(b)) for a close-up on a roll spacing. Local temperature drops beneath the rolls of slightly more than 100 K are produced from a typical f_{roll} value of 0.36. Local drops beneath each spray-nozzle impingement region vary from 30 K to 80 K according to the spray zone conditions.

The shell thickness predicted by the model (based on the solid fraction of 0.7) is also shown in Figure 7(a). Note that the entire cross section is solid just prior to the exit from the roll support region, which is consistent with plant experience for these conditions. The predicted temperatures generally exceed those measured by the pyrometers, except for the last pyrometer, which is outside the spray chamber and expected to be the most reliable. The difference is believed to be caused by the pyrometers reading lower than the real temperature, owing to steam-layer absorption and surface emissivity problems. Additional calibration work is needed to improve the accuracy of the pyrometer measurements, the spray heat-transfer coefficients, the spray-zone lengths, and the predicted variations in surface heat transfer and temperature to improve the agreement.

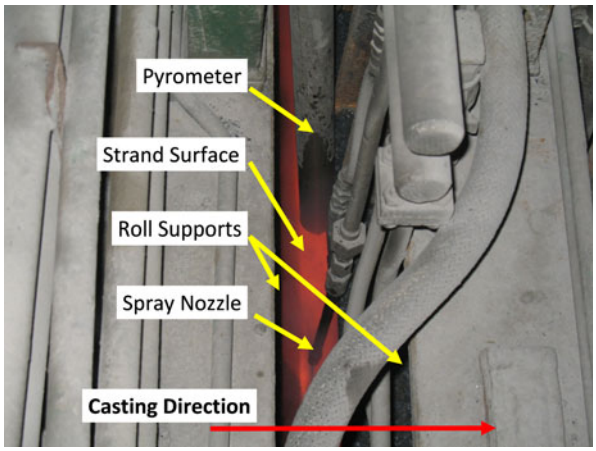

Fig. 6—Pyrometer arrangement in the Nucor south caster.

B. *Software Sensor—CONSENSOR*

The function of the software sensor is to predict the temperature distribution accurately in the strand in real time. The program CONSENSOR was developed to produce the temperature profile along the entire caster (z) and through its thickness (x) in real time (t), by exploiting CON1D as a subroutine. It does this by managing the simulation of N different CON1D slices, each starting at the meniscus at a different time to achieve a fixed z-distance spacing between the slices. This scenario is illustrated in Figure 8 using $N = 10$ slices for simplicity.

The control algorithm requires that CONSENSOR provide an updated surface-temperature estimate $\hat{T}(z,t)$ every Δt seconds. Note that the coordinates for T_i in CON1D slices (distance through thickness and time) are not the same as the coordinates for $\hat{T}$ in CONSENSOR (distance from meniscus and time). The surface-temperature

Table III. Spray Zone Input Values for CON1D Simulation of Experimental Case Conditions

Spray Zone	# of Rolls	Roll Radius (m)	Roll Pitch (m)	Spray Length (m)	Spray Width (m)	f_{roll}	$Q_{sw,j}$ (L/min/row)
1	1	0.062	0.090	0.05	1.640	0.01	79.8
2	5	0.062	0.165	0.05	0.987	0.08	188.0
3	6	0.062	0.177	0.05	0.987	0.22	123.0
4	5	0.070	0.189	0.05	1.008	0.20	50.6
5	10	0.080	0.213	0.05	1.620	0.36	50.6
6	10	0.095	0.236	0.05	1.680	0.36	26.0
7	12	0.095	0.249	0.05	1.680	0.36	47.4

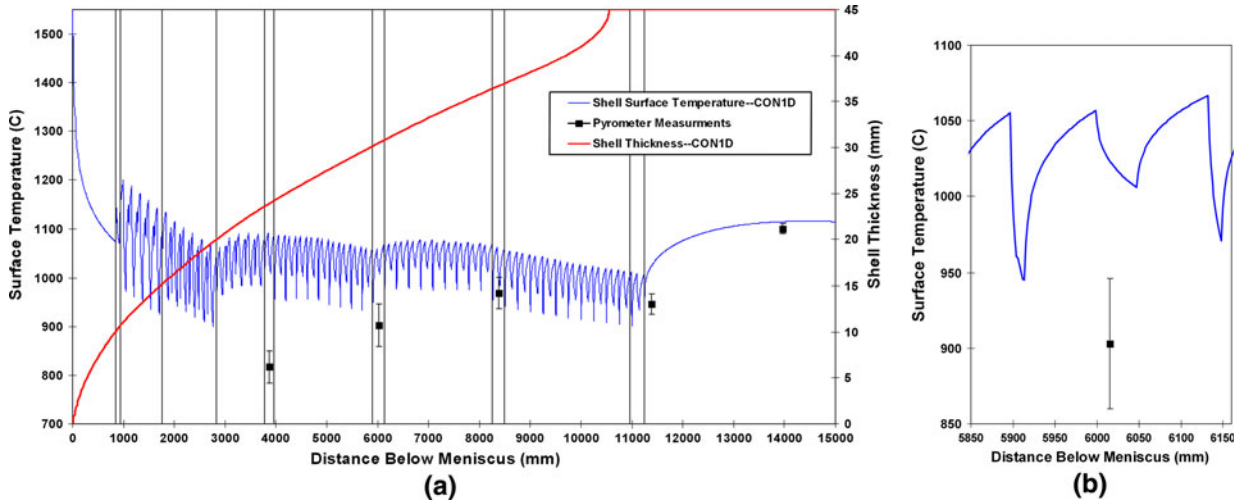

Fig. 7—Strand surface-temperature comparison of CON1D predictions and pyrometer measurements (*a*) along the entire domain and (*b*) close up near one roll spacing.

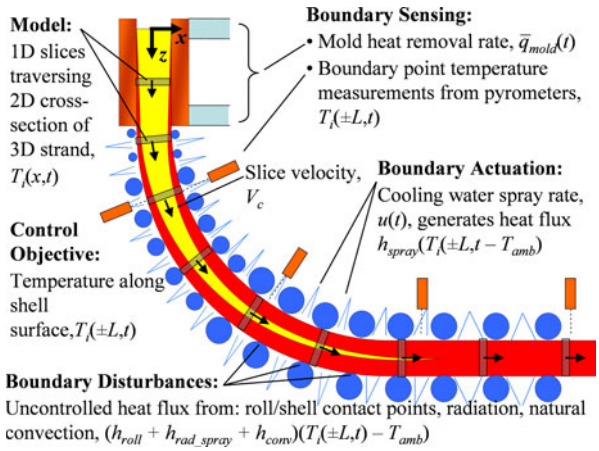

Fig. 8—CONSENSOR simulation domain.

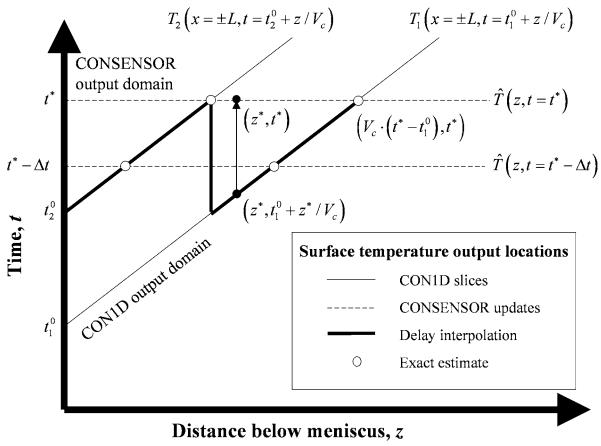

Fig. 9—Illustration of incremental runs of CON1D and the shell surface-temperature profile approximation using multiple slices with delay interpolation.

estimate $\hat{T}$ is assembled from the slice profile histories T_i as follows.

During each time interval, the N different CON1D simulations track the evolution of temperature in each slice over this interval, given the previously calculated and stored temperature distributions across the thickness of that slice at the start of the interval. The computation time required is approximately the same as just one complete CON1D simulation of the entire caster length, which takes about 0.6 seconds on the CentOS workstation when casting at 4.5 m/min.

During program startup, the simulation for slice $i+1$ begins when slice i passes 75 mm from the meniscus. After start-up, a new slice begins immediately from the meniscus whenever a slice reaches the end of the caster. Currently, CONSENSOR always manages exactly 200 slices, which corresponds to a uniform spatial interval of 75 mm along the caster length z_c, which is 15 m. The complete temperature history for each slice is stored from when it started at the meniscus t_i^0 to the current time t. To assemble the complete temperature profile needed, each time interval requires careful interpolation of the results of each slice at different times.

When plotted on a 2-D t-z grid, the desired output domain of the software sensor is a horizontal line, as shown in Figure 9. For instance, at time t^*, the sensor must predict $\hat{T}(z,t^*)$ for the entire caster length $0 \le z \le z_c$. However, the surface temperature included in a single slice history from CON1D traverses a monotonic-increasing curve in the t-z plane. At constant casting speed V_c, these curves are straight diagonal lines with slope of $1/V_c$. Figure 9 shows two such lines representing two slices created at times t_1^0 and t_2^0. It is clear from Figure 9 that each complete run of CON1D contributes only one data point to the desired software sensor output at each time, for example, $\hat{T}(z_i(t^*),t^*)$, where $z_i(t)$ is the location of the ith slice at time t, which is calculated as follows:

$$z_i(t) = \int_{t_i^0}^{t} V_c d\tau, \quad i = 1,2,\ldots 200 \qquad [12]$$

With constant casting speed, this integral simplifies to $V_c \times (t - t_i^0)$ (Figure 9). Data points in the temperature

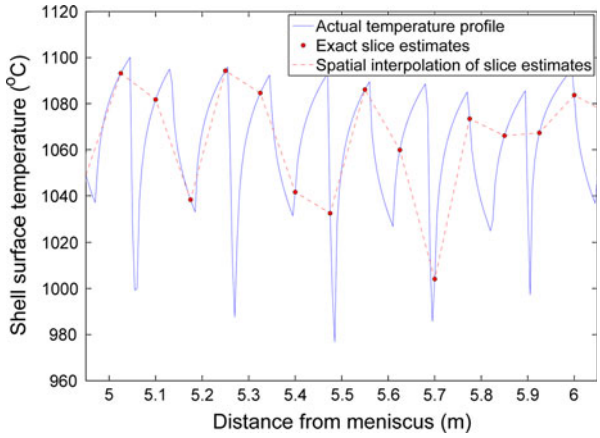

Fig. 10—Example of the actual temperature profile, the exact estimates, and spatially interpolated temperature profile.

profile estimate such as $\hat{T}(z_i(t^*), t^*)$, which come directly from CON1D output, are *exact* estimation points.

Figure 10 illustrates the error introduced by interpolating spatially between these exact points. The 75-mm span between slices in this work can pass over the temperature dips and peaks caused by the roll and spray spacing, resulting in errors of 100 K or more. This problem is overcome by "delay interpolation," interpolating temporally between the latest temperature histories available from each CON1D slice, described as follows and illustrated in Figure 9 using $N = 2$ slices.

For locations between the exact estimate points, the surface temperature is approximated at the current time using the most recent available temperature at that location from the CON1D slice histories. Applying this method everywhere along the caster, the control-oriented shell surface-temperature profile prediction $\hat{T}(z, t)$ is obtained as follows at any time t:

$$\hat{T}(z,t) = T_i(x = \pm L, t = t_i(z)) \text{ where } z_{i+1}(t) < z \leq z_i(t) \quad [13]$$

where $z_i(t)$ is given in Eq. [12], and $t_i(z)$ is the time at which the ith slice was the distance z from the meniscus, which is the inverse of Eq. [12] and expressed as follows:

$$t_i(z) = t_i^0 + \int_0^z \frac{d\zeta}{V_c} \quad [14]$$

For constant casting speed, this equation simplifies to $t_i^0 + z/V_c$. Figure 9 illustrates this process at time t^*. Starting from the previous time ($t^* - \Delta t$), the exact shell surface-temperature estimates are known at the previous locations of the two slices. The simulation restarts for each slice and continues for the desired time interval Δt giving temporally exact estimates at two new locations at time t^*. The point (z^*,t^*) lies in between the locations of these exact estimates, so according to the delay interpolation scheme, the surface temperature at this point is approximated by the surface temperature of slice 1 when it passed the distance z^* from the meniscus. Thus, the temperature $T_1(\pm L, t_i^0 + z^*/V_c)$ from the history of slice 1 is used to estimate the surface temperature $\hat{T}(z^*, t^*)$.

The approximation error introduced at location z^* in Figure 9 is the temperature change at this location from time $t_1(z^*)$ to $t^* + \Delta t$, which is a function of the extent of transient effects in the laboratory frame and slice spacing. It follows that slices should be distributed evenly to minimize the approximation error and that the magnitude of this error decays to zero during steady operation. Even during times of extreme transients, this error is easily recognized by operators from the jagged appearance of the temperature profile as it jumps from locations with the worst delays to the exact points. Note that the interpolation delay for the point (z^*,t^*) in Figure 9 is greater than the time interval (*i.e.*, $t_1(z^*) < t^* - \Delta t$). This case develops for some points when the slices travel less than the slice spacing during the time interval. During operation, the distance simulated during each time interval increases with casting speed but is usually less than the distance between slices. Specifically, the 75-mm span in this work is achieved only for speeds of 4.5 m/min or more. At lower speeds, the points further along each jag in the casting direction are most accurate because they contain the most recent temperature estimates.

C. *Control Algorithm—CONCONTROLLER*

Because heat transfer between slices is negligible, decentralized single-input–single-output controllers, which have no intercontroller interaction, can be used to control the spray-water flow rates to minimize the error between the CONSENSOR prediction and the set-point temperature profile. A single multi-input–multi-output controller is another option, but it is more complicated to design and implement and does not offer much better performance.

The temperature control problem can be regarded as a disturbance rejection problem in which the heat flux from the liquid core at the liquid–solid interface inside the strand can be treated approximately as a constant disturbance and the control goal is to maintain shell surface temperature under this disturbance. In light of this observation, the control law is simply chosen as the standard PI control. Here, the integral part is necessary for maintaining the surface temperature with no steady-state error under a constant set point and rejecting constant disturbances. Derivative control, which is normally introduced to increase damping and stability margin, is not used because the system itself is well damped, owing to the high thermal inertia of the solidifying steel strand.

An important feature of the caster spray configuration is that the rows of individual spray nozzles are grouped into N_{zone} spray zones according to nozzle location and control authority (which depends on how nozzles are connected *via* headers and pipes to a given valve). Each individual spray zone corresponds to an area in which the spray water to the nozzles has a single inlet valve. This means that all rows of nozzles in a zone have the same spray-water flow rate and spray density profile. This configuration is shown in Figure 11 and is

listed in Table IV, where u_j refers to the jth spray zone.[32] High in the caster, where the strand is vertical, nozzles on the inner and outer radii are part of the same spray zone, so they must be given the same spray flow rate command. For the caster in this work, this is the case for the first four spray regions. The lower three zones each have a separate zone and spray command for the inner and outer radius surfaces. Therefore, a total of $N_{\text{zone}} = 4 + 2 \times 3 = 10$ independent PI controllers are needed. The parameters of each controller are tuned separately to meet the control performance in each zone and are listed in Table V. These gains were chosen by assigning initial values based on the average total water flow through each zone and then tuning by trial and error based on experience obtained *via* offline simulations. CONONLINE provides model-based control only for the center-line zones. Based on these ten control signals, the spray flow rates for other zones across the strand width are prescribed as a function of slab width using separate logic. Generally, the flow rates per unit area are kept constant across the width, except in zones containing strand edges, where they are turned down slightly to lessen overcooling of the slab corners.

In accordance with this spray area configuration, the control algorithm proceeds through the following steps (Figure 3). At each time t, the inner and outer radii shell surface-temperature profile estimate $\hat{T}(z,t)$ is obtained by the software sensor as the multislice temperature calculation aggregated by means of the interpolation procedure illustrated in Figure 9. The desired shell surface-temperature profile set points are represented as $T^s(z,t)$ and are discussed in Section IV–F.

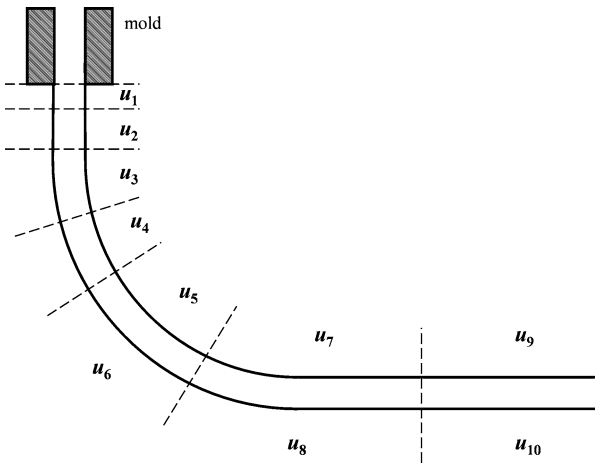

Fig. 11—Center spray zones configuration.

1. Calculate the average tracking error for each zone as follows:

$$\Delta T_j(t) = \frac{\int_{\text{zone}\,j} \left[\hat{T}(z,t) - T^s(z,t)\right] dz}{L_j}, \quad j = 1, \ldots, n_{\text{zone}} \qquad [15]$$

where L_j denotes the total length of zone j. In the upper caster, where the spray zones cover both sides of the strand, the integral is over both sides, and L_j is consequently twice the physical length of the strand in that zone.

2. Calculate the spray-water flow rate command for the next time interval, *via* the following classic PI control law:

$$u_j^P(t + \Delta t) = u_j^P(t + \Delta t) + u_j^I(t + \Delta t), \quad j = 1, \ldots, n_{\text{zone}} \qquad [16]$$

where the proportional and integral components are defined as follows:

$$u_j^P(t + \Delta t) = k_j^P \Delta T_j(t), \quad j = 1, \ldots, n_{\text{zone}} \qquad [17]$$

$$u_j^I(t + \Delta t) = u_j^I(t) + k_j^I \Delta T_j(t) \Delta t, \quad j = 1, \ldots, n_{\text{zone}} \qquad [18]$$

where Eq. [18] is a discrete-time integral over the time interval Δt, (1 second). The proportional and integral gains for each controller, k_j^P and k_j^I, respectively, are given in Table V.

Table V. Controller Gains

Controller	k^P	k^I
1	0.4	0.4
2	2.0	1.0
3	1.2	0.6
4	0.5	0.4
5–6	5.0	0.125
7–8	5.0	0.5
9–10	1.8	0.8

Table IV. Controller Assignments[32]

Spray Zone	Segment	Side	w_j (m)	l_j (m)	L_j (m)	Controller
1	foot rolls	both	1.640	0.05 × 2	0.090 × 2	u_1
2	upper bender	both	0.987	0.25 × 2	0.827 × 2	u_2
3	lower bender	both	0.987	0.30 × 2	1.061 × 2	u_3
4	segment 1	both	1.008	0.25 × 2	0.946 × 2	u_4
5	segment 2/3	inner	1.620	0.50	2.130	u_5
		outer	1.620	0.50	2.130	u_6
6	segment 4/5	inner	1.680	0.50	2.356	u_7
		outer	1.680	0.50	2.356	u_8
7	segment 6/7	inner	1.680	0.60	2.986	u_9
		outer	1.680	0.60	2.986	u_{10}

Note that Eq. [18] is a recursive definition; therefore, the initial settling time of the PI controller will depend on the initial choice of the control output $u_j^I(0)$ supplied when the control algorithm begins its calculations. During casting startup, PI control starts in a given zone only after steel has filled the zone entirely. Before this time, control is chosen based on the spray–table control method described in Section IV–F. When the PI control calculation begins for zone j, the spray-water flow rate from the spray-table is assumed as an initial value of u_j^I to reduce the initial settling time.

The control command $u_j(t)$, which is the requested water flow rate to spray zone j in L/s, is sent to the caster automation systems. The flow rate through the valve governing spray zone j, $u_j'(t)$, is measured by the caster automation systems and sent to CONSENSOR to estimate the surface heat flux using Eq. [9]. The spray-water flux used in Eq. [9] is currently assumed uniform over the nozzle footprints in each zone and is calculated as follows:

$$Q_{sw,j}(t) = \frac{u_j'(t)}{L_{\text{spray},j} w_j} \qquad [19]$$

where $Q_{sw,j}$ is the spray-water flux from each row of nozzles in zone j, w_j is the width, and $L_{\text{spray},j}$ the total length of the area of the steel surface on which all sprays in zone j impinge. The dimensions (Table IV) differ between spray zones according to how the distribution headers are constructed.

Finally, classical antiwindup[16] is adopted to avoid integrator windup when the transient control commands fall outside the range of feasible spray rates. Because of the physical limitations of the spray cooling system at the caster, it is common that the instantaneous spray rate requested by the control logic $u_j(t)$ exceeds the maximum or is less than the minimum limit achievable by the nozzles, so the measured spray rate $u_j'(t)$ is different. The requested and measured spray rates also may be different because of dynamics such as actuator interactions with the header piping system. These differences tend to cause controller instability, known as "windup." This problem is prevented by subtracting the difference from the integral portion of the control command, $u_j'(t)$ as follows[16]:

$$u_j^I(t+\Delta t) = u_j^I(t) + k_j^I \Delta T_j(t) \Delta t + k_j^{aw}\left(u_j'(t) - u_j(t)\right), \quad j = 1, \ldots, n_{\text{zone}} \qquad [20]$$

where k_j^{aw} is a tuning parameter that can be used to relax the rate of windup. Here, these parameters are set to 1. The computational closed-loop diagram in Figure 3 shows this antiwindup scheme graphically.

D. *Combining CONSENSOR and CONCONTROLLER—Certainty Equivalence and Loop Closure Issues*

The proportional–integral bank in the CONCONTROLLER system developed here uses strand surface temperature in the secondary cooling region estimated by an observer (CONSENSOR model program) to define its output error—deviation from the desired temperature-profile set points. In control terminology, this is the "certainty equivalence principle," or using the estimate as if it were the true value.

The loop closure employed here, however, has some special features. In the mold, CONSENSOR performs closed-loop estimation, with the temperature estimate being accurate because it is based on the measured mold heat removal rate and an accurate boundary heat flux profile (*cf.* Section IV–A–1 and Figure 3). The estimated slice temperature profile at the mold exit, denoted by $T_i(x, t_i^0 + t_m)$ in Figure 3, is referred to as an inferred measurement[33] because it is produced by a model from a secondary measurement. Because of the temperature continuity at mold exit, this inferred measurement becomes the initial condition for the slice prediction in the secondary cooling region. Hence, at the start of the secondary cooling region, the control system achieves inferential closed-loop control.

In the rest of the secondary cooling region, reliable real-time heat-transfer measurements are not possible, so the controller uses open-loop model-based temperature estimates. The quality of these estimates is still good because, in addition to being accurately initialized at mold exit, the model correctly incorporates the effects of several casting process changes (with casting speed, superheat, and grade being the most important) on strand-temperature evolution from a fundamental basis and has been calibrated offline to predict whale formation correctly under a few typical conditions. However, several other process variations, such as hysteresis in the boiling heat-transfer coefficients and spray-nozzle clogging, are not modeled in CONSENSOR. Without the ability to measure the strand surface temperature accurately and robustly in real time, surface temperature estimate accuracy could deteriorate with distance below the mold exit.

This combination of closed-loop estimation localized at mold exit (*i.e.*, spatially discrete) with open-loop estimation throughout the rest of the strand (*i.e.*, spatially continuous) is strictly termed a hybrid discrete-continuous[34] closed-loop/open-loop observation of the strand temperature profile in the secondary cooling region. The resulting control system thus can be termed hybrid closed-loop/open-loop system as well. Even if the placement of reliable pyrometers becomes technically feasible in the future, the pyrometer measurements are still essentially spatially discrete, and strand temperature in the gaps between pyrometers would have to be estimated in the open loop. Hence, the control system would retain this hybrid nature. Because this strategy reinforces the importance of modeling accuracy to ensuring estimator quality, lab measurement of heat-transfer coefficients during air-mist spray cooling and additional calibration with plant measurements are being addressed as other important aspects of the larger project.

E. *Visualization—Monitor*

Although not an element of the control diagram in Figure 1, the monitor is an important component in the control system because it provides real-time display of many variables, set points, and results, permitting

operators and plant metallurgists to monitor the caster and the control system performance as well as to make adjustments as needed. In addition to the instantaneous casting conditions, the monitor displays, for both the outer and the inner radii, the estimated shell surface-temperature profiles, the corresponding temperature set points in each zone, the estimated shell thickness growth profile, the controller-requested water flow rates control commands in each zone, the corresponding measured flow rates, and other parameters. To avoid network traffic problems, the refresh rate on the monitor is 3 seconds.

Figure 12 shows typical screen shots of both monitor interface windows. Figure 12(a) shows the "profile screen." This screen serves two purposes. The first purpose is to relay key simulation outputs to the operators and plant engineers. Important caster parameters such as casting speed and the final solidification point are noted at the top of the screen. The two opposing shell profiles form a V-shape that looks like the real liquid pool. Together with the superimposed temperature profiles, it is easy to visualize the state of the caster. The second purpose of the profile screen is to supply an interface for operator input to the controller *via* a drop-down box of set-point generation options and individual controls to change the temperature set point in any zone manually. The controller can generate temperature set points in several ways, as described in the next section. Figure 12(b) shows the "parameter screen," which displays the most important caster measurements input to the model. This setup allows for easy checking of the casting conditions as well as TCP/IP server and client operation.

The importance of the monitor as part of the control system should not be underestimated. By presenting accurate information to the operator in real time in a natural visual manner, this system empowers the operator to react better to unforeseen situations. Ultimately, a truly "expert" caster control system should recognize and take appropriate action to prevent potential problems in addition to controlling sprays to maintain surface temperature.

F. *Set-Point Generation*

Choosing good set points for spray cooling is as challenging and important as the control task itself. Several different methodologies are explored in this work. The current (old controller) spray practice is based on "spray-table control." The spray flow rates in each zone down the caster, or "spray pattern," that produce good quality steel for a specific group of steel grades in a specific caster are determined from plant trial and error and previous experience. Higher casting speed requires higher water flow rates to maintain the same cooling conditions (see Table VI for typical spray practices used in this work). Thus, for each spray pattern, a different spray profile is tabulated for each casting speed in a grid (database) that spans the range of normal operation. During casting, spray set points are interpolated from the appropriate spray-table database for the chosen pattern, according to the current casting speed. This method has the disadvantage that it does not accommodate transient behavior in the strand.

Previous theoretical knowledge on optimizing spray cooling is defined in terms of steady-state surface-temperature profiles to avoid various embrittlement and cracking problems that are associated with particular temperature ranges.[2] Furthermore, surface-temperature variations with time, such as those that occur during speed changes, startup, and tailout, are detrimental because they cause surface stress and defects. To combine these two types of knowledge, the spray tables were converted to tables of surface-temperature profile set points. As shown in Figure 3, this is a two-step process comprising the generation of set-point profiles offline and the interpolation of these profiles during casting. To generate the set points, CON1D was run for every casting speed and all patterns according to the tabulated spray profiles. The resulting temperatures are stored in a 2-D array (according to speed and pattern). During operation, these profiles are interpolated to find the desired temperature profile for the current casting speed and pattern to use as the set point for the PI controller $T^s(z,t)$. This second approach is referred to as "speed-dependent temperature set points."

However, the temperature set points do not need to vary with casting speed during operation. If the computational model is reliable, then it is better to use a constant temperature set point for all casting speeds. In this work, a representative profile was chosen from each pattern in the speed-dependent temperature–set-point database, reducing the set-point table by one dimension. This approach takes advantage of the fact that steel thermal properties are relatively independent of steel grade and casting speed, so that quality depends mainly on the surface-temperature profile.

During offline (shadow mode) plant testing, the controller output using fixed temperature set points called for many sharp changes in spray rate in the first few spray zones. It was discovered that this was caused by significant variations in the strand surface temperature at the mold exit with changes in the mold heat flux, casting speed, and steel grade. Forcing the surface temperature to change quickly to a specified temperature set point causes detrimental sharp changes in the shell surface temperature, especially in the first two spray zones below the mold. Such changes, and the associated thermal stresses, are what set-point-based control is supposed to avoid.

The root of the problem is that temperature profiles are sensitive to the mold heat flux, which is not accounted for in the spray table. To generate the set points, the average mold heat flux needed for Eq. [3] $\bar{q}_{\text{mold}}$ was estimated as a function of mold powder and casting speed from the following empirical correlation[35]:

$$\bar{q}_{\text{mold0}} = 4.63 \times 10^6 \mu^{-0.09} T_{\text{flow}}^{-1.19} V_c^{0.47} \times \left(1 - 0.152 \exp\left[-\left(\frac{0.107 - \text{pct}C}{0.027}\right)^2\right]\right) \quad [21]$$

where $\bar{q}_{\text{mold0}}$ is the estimated average mold heat flux (MW/m^2), μ is the powder viscosity at

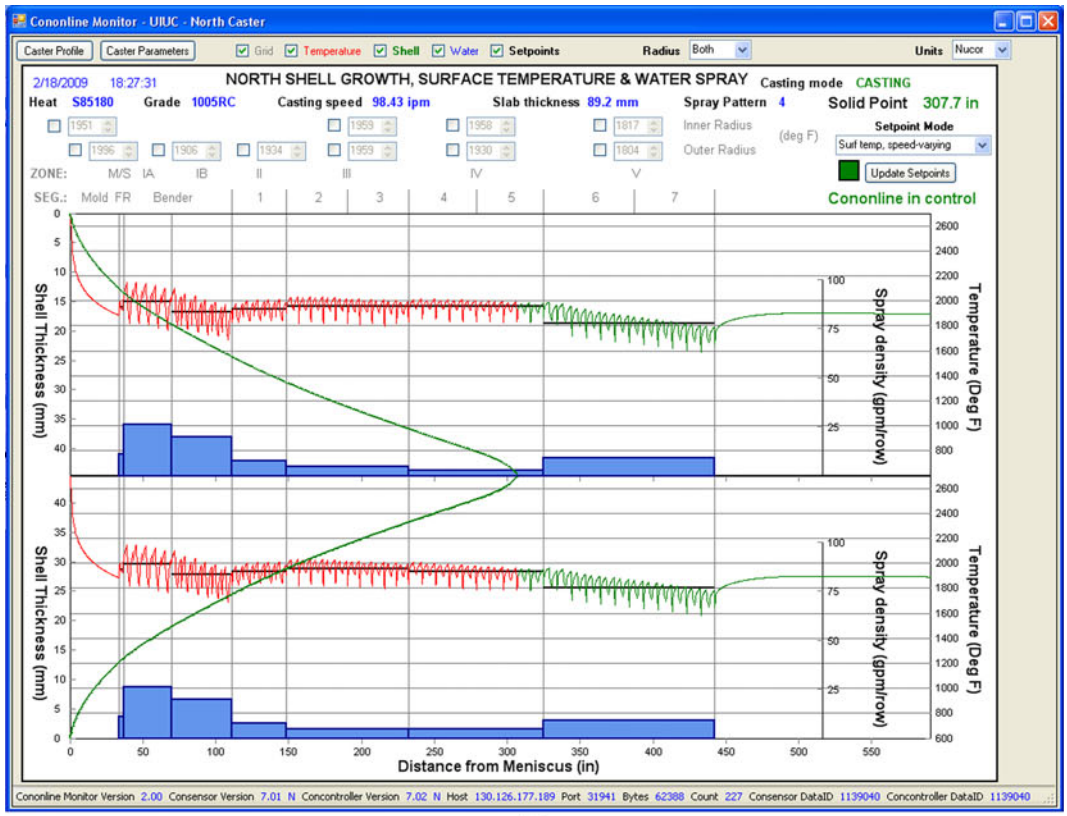

(a)

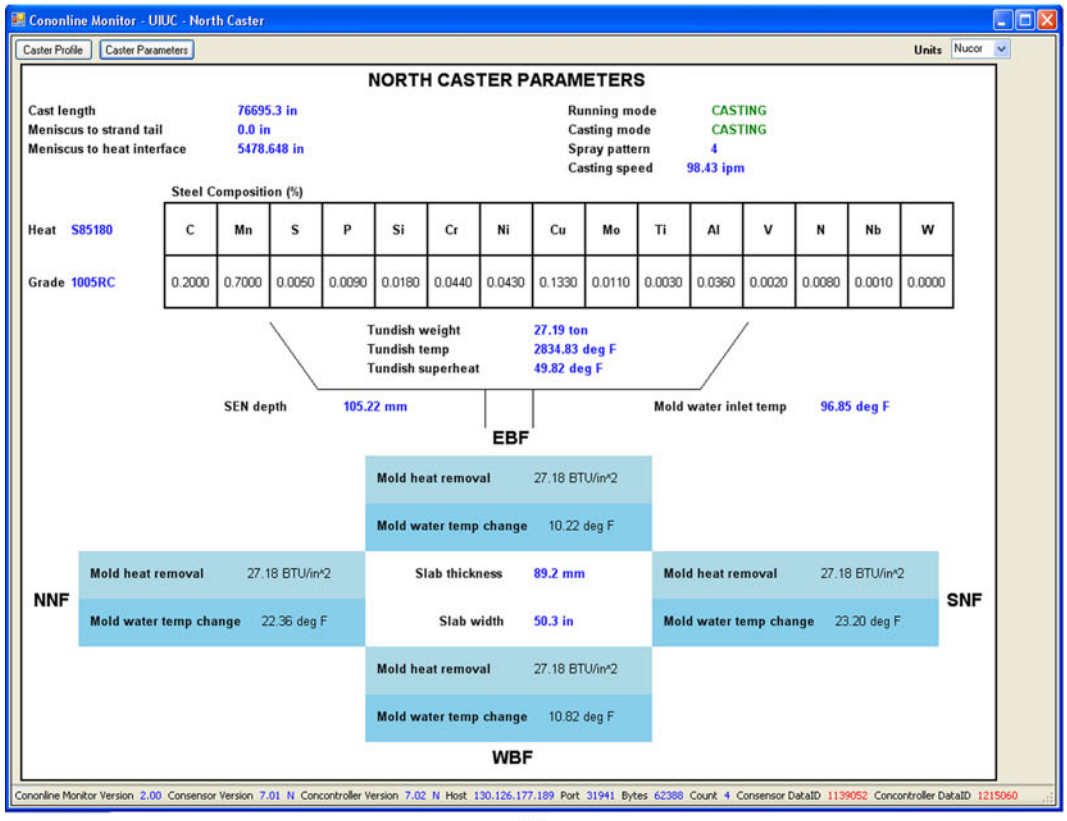

(b)

Fig. 12—CONONLINE Monitor interface example screens. (*a*) Profile screen showing strand surface temperature and shell thickness predictions, requested and achieved spray-water flow rates, controller set points, operator controls, and relevant caster data. (*b*) Parameter screen showing caster input data from caster automation systems, including steel composition and mold heat flux measurements.

Table VI. Nominal Spray Fluxes in Simulations

Controller	Q_{sw} at 3.0 m/min (L/s/m^2)	Q_{sw} at 2.5 m/min (L/s/m^2)
u_1	13.46	11.54
u_2	40.15	30.44
u_3	31.97	22.81
u_4	11.89	6.27
u_5	5.61	1.80
u_6	5.61	1.80
u_7	3.23	1.05
u_8	4.81	1.66
u_9	10.24	10.24
u_{10}	10.24	10.24

1573 K (1300 °C), (Pa s), T_{flow} is the melting temperature of the mold flux (°C), V_c is the casting speed (m/min), and pct$C$ is the carbon content (pct).

Even though this equation reasonably predicts mold heat flux at the caster in this work, (and could be tuned to be even better), the effects of unaccounted variables (such as mold powder changes, superheat effects, and random variations) always cause the measured mold heat flux as well as the corresponding surface temperature at the mold exit to change significantly with time at a given casting speed (set point).

To avoid this problem, a new set-point strategy, called "fixed temperature set points" was developed that allows the temperature profile set points to vary with mold heat flux and, consequently, with mold exit temperature. Five different temperature profile set-point curves are generated using CON1D with $0.7\bar{q}_{\text{mold0}}$, $0.85\bar{q}_{\text{mold0}}$, $\bar{q}_{mold0}$, $1.15\bar{q}_{\text{mold0}}$, and $1.3\bar{q}_{\text{mold0}}$. An example of the five temperature set-point curves for one particular pattern is shown in Figure 13. It is shown that these set points produce mold exit temperatures that span a wide range from 1123 K (850 °C) to 1523 K (1250 °C). This third strategy again stores a 2-D array of fixed temperature set points (organized according to mold heat flux and pattern).

During operation, these set points can be interpolated linearly against the mold exit temperature to choose a temperature set-point profile that includes a match with the current mold exit temperature. The effect of mold heat flux variations diminishes with distance down the strand, so the set point is allowed to vary with the mold exit temperature only in the first four zones. The temperature set point for the remaining zones uses the original fixed set point corresponding with $\bar{q}_{\text{mold0}}$. The impact of mold heat flux variations thus is evenly distributed over the first four spray zones and thereby avoids sharp spray rate changes and corresponding surface temperature changes in the first few spray zones.

The final (fourth) control strategy is to accept zone set-point temperatures from the operator through the monitor interface. The automatic set points can be overridden in any zone(s). Even with this strategy, however, manual control is not given to the first spray zone, which is simply fixed to avoid the problems previously mentioned.

In summary, the set points used by the online control system are organized in a 3-D array (according to pattern, speed, and mold heat flux), constructed prior to the start of operation. Currently, the operator can choose any one of four control methods. The first is "spray-table control," which mimics the current (old) control method of choosing sprays based simply on the current casting speed and grade. The second is "speed-dependent set points," in which temperature set points are generated from the spray table and are interpolated based on casting speed. The third is "fixed set points," in which temperature set points are interpolated based on the mold exit temperature. In the fourth method, set points are input directly by the operator, overriding automatic set-point generation in any given zone. The simulations in the next section examine the performance of these different set point methodologies.

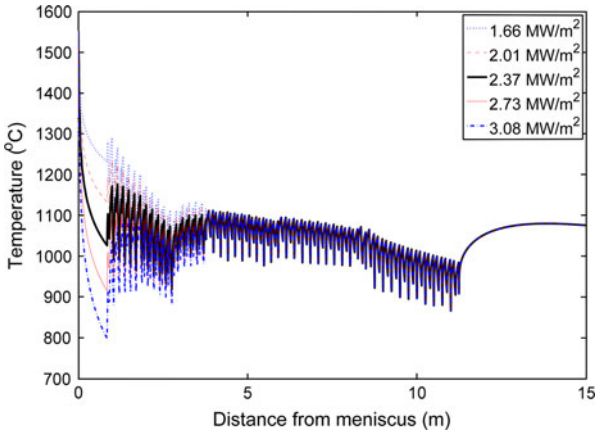

Fig. 13—The five temperature set-point curves for spray pattern 4 with varying mold heat removal rates.

V. EXAMPLE SIMULATION RESULTS

The model and controller programs can be used to simulate the caster response to scenarios involving changing casting conditions. Using the monitor, the results even can be viewed graphically in real time. Initial efforts have focused on evaluating the control system performance, especially comparing the old control system of fixing spray-water flow rates with casting speed with the two different options for set-point interpolation of the new controller. For example, Figure 14 compares the zone-average surface-temperature histories extracted from the software sensor predictions in spray zones 2 and 8 during a sudden drop in casting speed from 3.0 m/min to 2.5 m/min at $t = 30$ seconds, with an accompanying drop in mold heat flux from 2.373 to 2.178 MW/m^2. Figure 15 shows the respective spray rates assigned to each zone using the four different control methods. Zone 2 covers both sides of the strand, as shown in Figure 11, but only the average outer radius surface temperature is plotted in Figure 14. The simulations were run for the same conditions given in Section IV–A–3 and in Tables III, IV, and VI, except for a pour temperature of 1830 K (1557 °C).

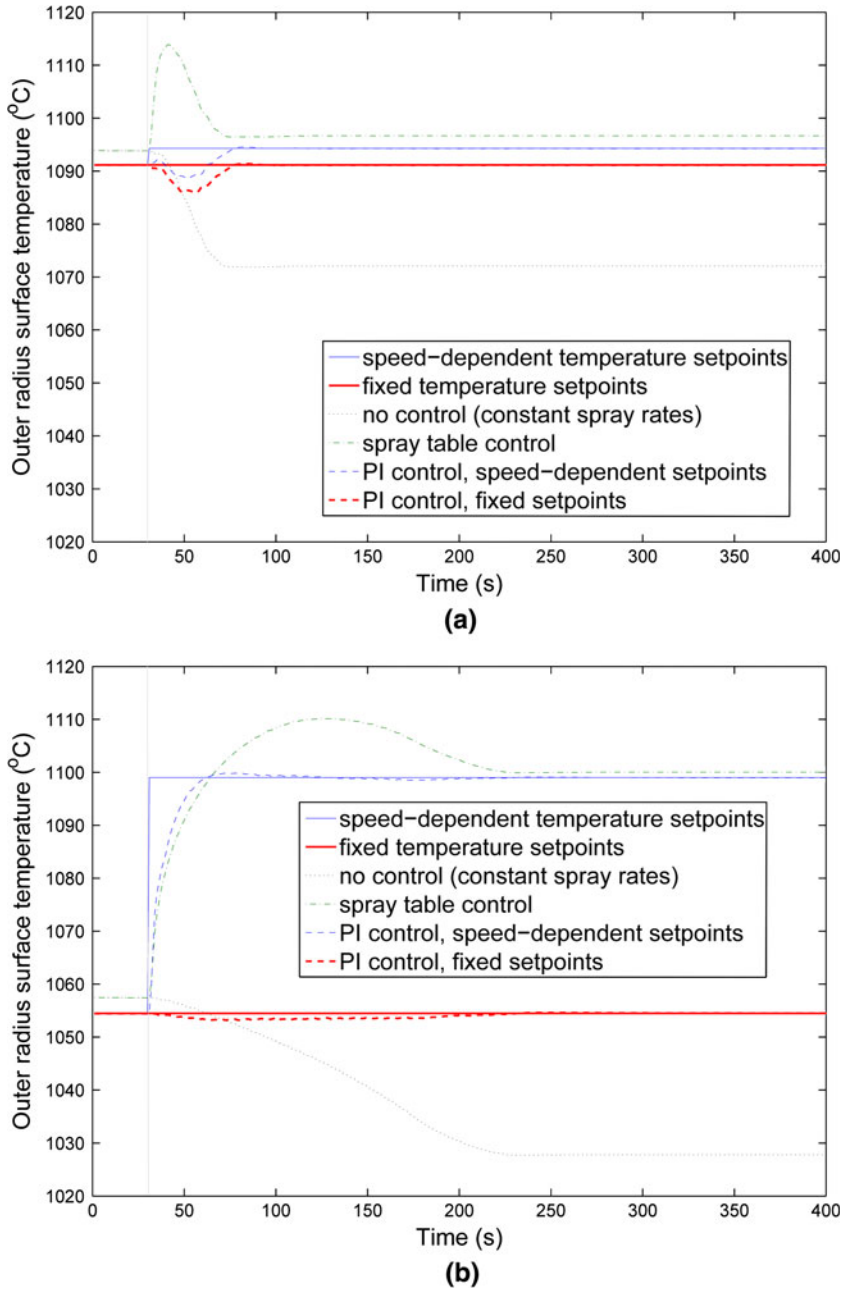

Fig. 14—Zone-average temperatures during a sudden slowdown from 3.0 to 2.5 m/min casting speed, comparing four control methodologies. (*a*) Spray zone 2 (outer radius). (*b*) Spray zone 8.

With no controller, spray-water flow rates remain constant with time, so the decrease in casting speed causes higher heat extraction at any given distance down the caster, and the surface temperatures all eventually drop. The time delay for the transition to the new lower steady-state temperature varies with distance down the caster. Steady state is not reached until steel starting at the meniscus at the transition time (t = 30 seconds) finally reaches the given point in the caster after being cast entirely under the new conditions. Thus, points nearer to the meniscus react quickly to the change, whereas points lower in the caster are affected by the changing upstream temperature history for a long time. In the figures, it is clear that zone 2 reaches steady state sooner than zone 8.

With a controller that increases spray water in proportion to casting speed, the responses in Figure 14 show a characteristic temperature overshoot before settling to steady state. During a sudden casting speed drop, the spray rates drop immediately, as shown in Figure 15. However, with the recently higher casting speed, the upstream steel is hotter than expected, so the surface temperatures overshoot the desired values at steady state. The steady-state temperatures at 2.5 m/min are larger than the steady-state temperatures at 3.0 m/min because the spray rates assigned at the lower speed

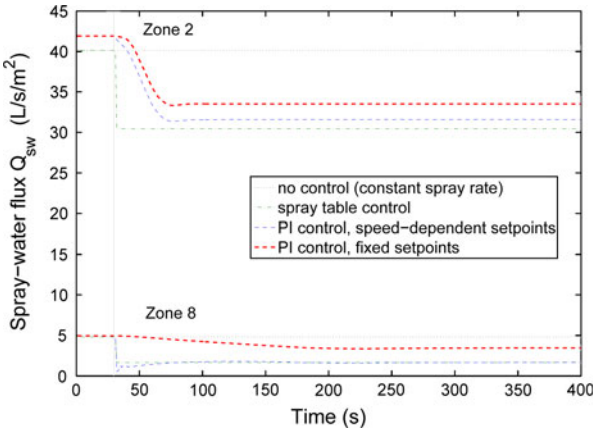

Fig. 15—Spray-water flow rates corresponding to Fig. 13 example during a sudden slowdown from 3.0 to 2.5 m/min casting speed, comparing four control methodologies.

are predicted by the model to be even lower than the drop in speed requires.

With PI control using speed-dependent temperature set points, the overshoot is drastically reduced. In fact, Figure 14(a), shows that a slight undershoot is initially present in zone 2. As Figure 15 makes clear, this is because the spray flow rate command from the PI controller changes more gradually than spray-table control. However, the command changes as sharply as the spray-table control in zone 8. This response is needed to achieve the larger change in temperature set points at the speed change.

Finally, these results illustrate the superiority of PI control using fixed temperature set points. With this controller, the surface temperature is kept remarkably constant through the speed change. To achieve this, Figure 15 clearly shows how the sprays are decreased gradually after the casting speed change, and the further the zone is from meniscus, the more gradually the spray rate is changed. The steady-state spray-water flow rates are properly smaller at the lower casting speed.

This case study demonstrates that all controllers perform as expected. The PI controller with fixed set points produces the best response for steel quality, as detrimental surface-temperature fluctuations are lessened. The quality of the control system now depends on the accuracy of the software sensor calibration to match the real caster. Work is proceeding to measure heat transfer, both with fundamental laboratory experiments and with optical pyrometers and other experiments in the commercial steel thin-slab caster.

VI. SUMMARY

Maintaining the shell surface-temperature profile under transient conditions by spray-water cooling in continuous casting of steel is important to minimize surface cracks. For this purpose, a real-time spray-cooling control system, CONONLINE, is being implemented on a commercial caster that includes (1) a software sensor for accurate estimation/prediction of shell surface temperature; (2) control algorithm and data-checking subroutines for robust temperature control; (3) TCP/IP server and client programs for communicating between these two software components and the caster; and (4) a real-time monitor to allow operator input and display the predicted shell surface-temperature profiles, water flow rates, and other important operating data. Simulation results demonstrate that the new control system achieves better temperature control performance than conventional systems, especially when using a new strategy to generate temperature set points that vary according to the measured mold heat flux and a controller with antiwindup that maintains a constant surface-temperature profile with casting speed.

ACKNOWLEDGMENTS

Ron O'Malley, Matthew Smith, Terri Morris, and Kris Sledge from Nucor Decatur are gratefully acknowledged for their unwavering support and help with this work. The TCP/IP programs in CONONLINE were written by Rob Oldroyd from DBR Systems on behalf of Nucor Decatur. We are grateful for work on CON1D calibration for the Nucor Decatur steel mill by Sami Vahpalahti and Huan Li from the University of Illinois. We are also very grateful for their work on CONONLINE. This work is supported by the National Science Foundation under Grants DMI 05-00453 and CMMI-0900138 as well as the Continuous Casting Consortium at UIUC.

NOMENCLATURE

^{0}	superscript to indicate initial time of creation (at meniscus)
Cp^*_{steel}	effective specific heat of steel, including latent heat of solidification (J/kg K)
Δt	time interval for control calculation (s)
Δt_{FD}, Δx	time step (s) and grid spacing (m) used in CON1D explicit finite difference scheme
ΔT_j	difference between estimated average surface temperature and set point in zone j (°C)
f_{roll}	fraction of heat removed through roll contact in zone
i	subscript for CON1D slice number, used in CONSENSOR (N total)
j	subscript for spray zone number (N_{zone} total)
k_j^P, k_j^I, k_j^{aw}	proportional, integral, and antiwindup controller gains
k_{steel}	thermal conductivity of steel (W/m K)
L_j	total length of zone j (m)
$L_{\text{roll contact},j}$	length of zone j in which rolls are in contact with the steel surface (m)
$L_{\text{spray},j}$, w_j	length and width of the area of the steel surface upon which all the sprays in zone j impinge (m)
n_{pattern}	index denoting desired spray pattern

p_E	weight percent of alloying element E
q	surface heat flux at a particular time and location (MW/m^2)
$\bar{q}_{\text{mold}}$	average steel surface heat flux in mold (MW/m^2)
$Q_{sw,j}$	spray water flux ($L/s/m^2$) on surface of steel in zone j
ρ_{steel}	density of steel (kg/m^3)
t	real time (s)
$t_i(z)$	time when slice i passes distance z from the meniscus (s)
$T_i(x,t)$	temperature of CON1D slice i: 1-D transverse cross section moving along strand centerline at V_c (°C)
$T^s(z,t)$	strand surface-temperature set point (°C)
$\hat{T}(z,t)$	strand surface-temperature estimate (°C)
T_{amb}	ambient temperature (°C)
T_{pour}	measured temperature of molten steel in the tundish (°C)
T_{spray}	measured temperature of spray water (°C)
$u_j'(t)$, $u_j(t)$	spray water flow rate: measured, requested controller output (L/s)
$u_j^P(t)$, $u_J^I(t)$	proportional and integral portions of requested spray water flow rate (L/s)
V_c	casting speed (m/s)
x	distance through thickness of strand (m)
z	distance from meniscus, in casting direction (m)
$z_i(t)$	distance from meniscus of slice i at time t (m)
z_m	mold length (m)

REFERENCES

1. J.K. Brimacombe, P.K. Agarwal, S. Hibbins, B. Prabhaker, and L.A. Baptista: in *Continuous Casting*, J.K. Brimacombe, ed., 1984, vol. 2, pp. 105–23.
2. M.M. Wolf: *Continuous Casting: Initial Solidification and Strand Surface Quality of Peritectic Steels*, Iron and Steel Society, Warrendale, PA, 1997, vol. 9, pp. 1–111.
3. K. Okuno, H. Naruwa, T. Kuribayashi, and T. Takamoto: *Iron Steel Eng*., 1987, vol. 12 (4), pp. 34–38.
4. K.-H. Spitzer, K. Harste, B. Weber, P. Monheim, and K. Schwerdtfeger: *ISIJ Int*., 1992, vol. 32 (7), pp. 848–56.
5. S. Barozzi, P. Fontana, and P. Pragliola: *Iron Steel Eng*., 1986, vol. 11, pp. 21–26.
6. B. Lally, L. Biegler, and H. Henein: *Metall. Trans. B*, 1990, vol. 21B, pp. 761–70.
7. K. Dittenberger, K. Morwald, G. Hohenbichler, and U. Feischl: *Proc. VAI 7th International Continuous Casting Conference*, Linz, Austria, 1996, pp. 44.1–6.
8. R.A. Hardin, K. Liu, A. Kapoor, and C. Beckermann: *Metall. Mater. Trans. B*, 2003, vol. 34B, pp. 297–306.
9. S. Louhenkilpi, E. Laitinen, and R. Nienminen: *Metall. Mater. Trans. B*, 1999, vol. 24B, pp. 685–93.
10. S. Louhenkilpi, J. Laine, T. Raisanen, and T. Hatonen: *2nd Int. Conf. on New Developments in Metallurgical Process Technology*, Riva del Garda, Italy, 2004.
11. T. Raisanen, S. Louhenkilpi, T. Hatonen, J. Toivanen, J. Laine, and M. Kekalainen: *European Congress on Computational Methods in Applied Sciences and Engineering*, 2004.
12. M. Jauhola, E. Kivela, J. Konttinen, E. Laitinen, and S. Louhenkilpi: *Proc. 6th International Rolling Conference*, Dusseldorf, Germany, 1994, vol. 1, pp. 196–200.
13. K. Zheng, B. Petrus, B.G. Thomas, and J Bentsman: *AISTech 2007, Steelmaking Conf. Proc*, Indianapolis, IN, 2007.
14. B.G. Thomas, J. Bentsman, B. Petrus, H. Li, A.H. Castillejos, and F.A. Acosta: *Proc. 2009 NSF CMMI Engineering Research and Innovation Conference*, Honolulu, HI, 2009, p. 16.
15. Y. Meng and B.G. Thomas: *Metall. Mater. Trans. B*, 2003, vol. 34B, pp. 685–705.
16. C. Edwards and I. Postlethwaitex: *Proc. UKACC International Conference on CONTROL*, 1996, pp. 394–99.
17. B. Santillana, L.C. Hibbeler, B.G. Thomas, A. Hamoen, A. Kamperman, and W. van der Knoop: *ISIJ Int*., 2008, vol. 48 (10), pp. 1380–88.
18. J. Sengupta, M.-K. Trinh, D. Currey, and B.G. Thomas: *Proc. AISTech 2009 Steelmaking Conf. Proc*., St. Louis, MO, 2009.
19. Y.M. Won and B.G. Thomas: *Metall. Mater. Trans. A*, 2001, vol. 32A, pp. 179, 1755–67.
20. Y. Meng and B.G. Thomas: *Metall. Mater. Trans. B*, 2003, vol. 34B, pp. 707–25.
21. J.-K. Park, B.G. Thomas, I.V. Samarasekera, and U.-S. Yoon: *Metall. Mater. Trans. B*, 2002, vol. 33B, pp. 425–36.
22. T. Nozaki: *Trans. ISIJ*, 1978, vol. 18, pp. 330–38.
23. R.A. Hardin, H. Shen, and C. Beckermann: *Proc. Modelling of Casting, Welding and Advanced Solidification Processes IX*, Aachen, Germany, 2000, pp. 190, 729–36.
24. E. Mizikar: *Iron Steel Eng*., 1970, vol. 47, pp. 53–60.
25. L.K. Chiang: *Proc. 57th Electric Furnace Conf*., Pittsburgh, PA, 1999.
26. K. Tanner: in *Proc. MS&T Conf. Proc*, B.G. Thomas, ed., New Orleans, LA, 2004.
27. K. Kasperski: in *Proc. MS&T Conf. Proc*., B.G. Thomas, ed., New Orleans, LA, 2004.
28. S.-M. Lee and S.-Y. Jang: *ISIJ Int*., 1996, vol. 36, pp. 208–10.
29. S. Vapalahti, H. Castillejos, A. Acosta, A.C. Hernández, and B.G. Thomas: "Delavan Nozzle Characterization Research at CINVESTAV," CCC Report, #CCC0703, University of Illinois, June 12, 2007.
30. S. Vapalahti, H. Castillejos, A. Acosta, A.C. Hernández, and B.G. Thomas: "Spray Heat Transfer Research at CINVESTAV," CCC Report, #CCC0704, University of Illinois, June 12, 2007.
31. S. Vapalahti, B.G. Thomas, S. Louhenkilpi, A.H. Castillejos, F.A. Acosta, and C.A. Hernandez: *Proc. STEELSIM 2007*, Graz, Austria, 2007.
32. LLC Trico Steel: *Spray Nozzle Arrangement*, Cleveland, OH, 1995.
33. C. Brosilow and B. Joseph: *Techniques of Model-Based Control*, Prentice Hall, Upper Saddle River, NJ, 2002.
34. Y.V. Orlov and M.V. Basin: *IEEE Trans. Automat Contr*, 1995, vol. 40 (9), pp. 1623–26.
35. C. Cicutti, M. Valdez, T. Perez, G.D. Gresia, W. Balante, and J. Petroni: *Proc. 85th Steelmaking Conf*., Nashville, TN, 2002, vol. 85, pp. 97–107, 282.